THE JOURNAL OF PHYSICAL CHEMISTRY B

Article

pubs.acs.org/JPCB

Mechanism of Pyrogallol Red Oxidation Induced by Free Radicals and Reactive Oxidant Species. A Kinetic and Spectroelectrochemistry Study

E. Atala,[†] G. Velásquez,[‡] C. Vergara,[§] C. Mardones,[§] J. Reyes,[†] R. A. Tapia,[∥] F. Quina,[⊥] M. A. Mendes,[⊥] H. Speisky,[#] E. Lissi,[‡] M. S. Ureta-Zañartu,[‡] A. Aspée,*[,‡] and C. López-Alarcón*[,†]

[†]Departamento de Farmacia, Facultad de Química, Pontificia Universidad Católica de Chile

[‡]Departamento de Ciencias del Ambiente, Facultad de Química y Biología, Universidad de Santiago de Chile

[§]Facultad de Farmacia, Universidad de Concepción, Chile

[∥]Departamento de Química Orgánica, Facultad de Química, Pontificia Universidad Católica de Chile

[⊥]Instituto de Química, Universidad de Sao Paulo, Sao Paulo, Brazil

[#]Instituto de Nutrición y Tecnología de los Alimentos, INTA, Universidad de Chile

Supporting Information

ABSTRACT: Pyrogallol red (PGR) presents high reactivity toward reactive (radical and nonradical) species (RS). This property of PGR, together with its characteristic spectroscopic absorption in the visible region, has allowed developing methodologies aimed at evaluating the antioxidant capacity of foods, beverages, and human fluids. These methods are based on the evaluation of the consumption of PGR induced by RS and its inhibition by antioxidants. However, at present, there are no reports regarding the degradation mechanism of PGR, limiting the extrapolation to how antioxidants behave in different systems comprising different RS. In the present study, we evaluate the kinetics of PGR consumption promoted by different RS (peroxyl radicals, peroxynitrite, nitrogen dioxide, and hypochlorite) using spectroscopic techniques and detection of product by HPLC mass spectrometry. The same pattern of oxidation and spectroscopic properties of the products is observed, independently of the RS employed. Mass analysis indicates the formation of only one product identified as a quinone derivative, excluding the formation of peroxides or hydroperoxides and/or chlorinated compounds, in agreement with FOX's assays and oxygen consumption experiments. Cyclic voltammetry, carried out at different pH's, shows an irreversible oxidation of PGR, indicating the initial formation of a phenoxy radical and a second charge transfer reaction generating an ortho-quinone derivative. Spectroelectrochemical oxidation of PGR shows oxidation products with identical UV−visible absorption properties to those observed in RS-induced oxidation.

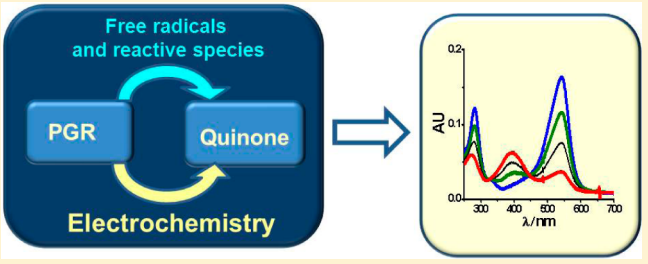

1. INTRODUCTION

The pyrogallolsulfonphtalein dye (pyrogallol red, PGR) has been employed in clinical and chemical research. In the first case, the uses are mainly focused to quantify proteins in human fluids,[1,2] while, in the second one, PGR has been employed to determine, by the cathodic stripping electrochemical technique, metals in complex samples.[3−6] In addition, the catalytic activity of osmium, molybdenum, and palladium on the oxidation of PGR promoted by hydrogen peroxide has been proposed as the basis of simple assays to evaluate these metals in biological samples.[7−9] PGR has also been described as a redox mediator at the glassy carbon electrode catalyzing the oxidation of hydrazine at the electrodic surface.[10]

The chemical structure of PGR (shown in Figure 1) presents three hydroxyl groups (able to chelate metals and to be oxidized) in an aromatic conjugated chromophore system. In aqueous solutions, at physiological pH 7.0, PGR shows a strong

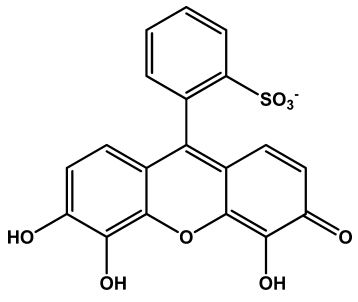

Figure 1. Chemical structure of PGR.

Received: January 14, 2013
Revised: March 20, 2013
Published: March 25, 2013

visible band (highly sensitive to the presence of metals or oxidants) with maximum absorbance at 540 nm. The formation of metal complexes with PGR, as well as its oxidation, can easily be followed by visible spectroscopy.[11]

In the last decades, PGR has also been employed as a probe in methodologies aimed to evaluate antioxidant capacity of foods, beverages, and human fluids.[11,12] In those studies, the consumption of PGR induced by several reactive species (RS), such as peroxyl radicals, peroxynitrite, hypochlorite, and superoxide, has been commonly followed by UV−visible spectroscopy.[13−16] Balavoine and co-workers reported that, among 14 tested target molecules, PGR was the best probe to assess scavenging activity of pure compounds toward peroxynitrite.[13] In addition, our research group has reported a convenient use of PGR as a probe in an ORAC (oxygen radical absorbance capacity)-like assay.[15] This latter PGR application requires simple instrumentation (since PGR consumption is followed at 540 nm) and allows obtaining an antioxidant capacity index associated with the quantity and reactivity of the free radicals removing compounds to react with peroxyl radicals. The method has been applied to determine the antioxidant capacity of pure compounds as well as tea, wines, fruit juices, and human plasma and urine, among others.[17−20] In addition, Niki and collaborators have proposed that the use of PGR and pyranine as probes gives complementary data regarding the scavenging activity of thiols, polyphenols, and complex samples toward peroxyl radicals.[19,21−23] In other context, the consumption of PGR mediated by superoxide has been employed to evaluate redox-cycling reactions of nitro-compounds mediated by rat liver microsomes.[14]

In spite of the above-mentioned studies and uses of PGR, to our knowledge, no reports regarding the mechanisms involved in its RS-induced oxidation have been published. Also, there are no reports on their electrochemical redox processes. Thus, in the present study, using spectroscopic and chromatographic techniques, we investigated the processes that lead to the oxidation of this dye during its reaction with different RS (i.e., peroxyl radicals, hypochlorite, nitrogen dioxide, and peroxynitrite). In addition, we present spectroelectrochemical evidence showing that the electrochemical oxidation of PGR leads to exactly the same spectroscopic behavior as that induced by the direct exposure of PGR to RS.

2. EXPERIMENTAL SECTION

2.1. Chemicals and Solutions. Pyrogallol red and 2,2′-azo-bis(2-amidinopropane) dihydrochloride (AAPH) were purchased from Sigma-Aldrich (St. Louis, MO). Hypochlorite was supplied by Merck (Darmstadt, Germany). All reagents were employed as received. In spectroscopic and chromatographic studies, solutions were prepared in phosphate buffer (75 mM, pH 7.4) using ultrapure water (Milli-Q) pretreated with Chelex-100 (1 g L^{-1}) for 12 h in order to remove metal traces. Electrochemical studies were carried out at room temperature with deaerated solutions prepared in 100 mM phosphate buffer, pH 7.4, using triple distilled water pretreated with Chelex-100 (1 g L^{-1}) for 12 h.

Peroxynitrite was synthetized according with the methodology described by Saha and co-workers.[24] Briefly, the reaction of hydrogen peroxide and sodium nitrite under acidic conditions was carried out employing a quenched-flow system. Excess hydrogen peroxide was removed with manganese dioxide, and peroxynitrite concentration was determined at 302 nm (ε = 1670 M^{-1} cm^{-1}). Stock solutions were stored at −80 °C and diluted in 0.1 M NaOH immediately before use.

To generate nitrogen dioxide, 10 mg of metallic copper was incubated at 25 °C with concentrated nitric acid (30 mL) in 20 mL of ultrapure water under constant stirring.[25] Nitrogen gas was employed as a carrier (at 45 mL min^{-1}). The nitrogen dioxide/nitrogen mixture was burbled into a spectroscopic cell containing PGR solutions (5−20 μM) in phosphate buffer 75 mM, pH 7.4, and the course of the reaction was followed at 540 nm. In the absence of either copper or nitric acid, no changes were registered in the UV−visible spectrum of PGR. In some experiments, aliquots (20 μL) of solutions were taken and injected into the HPLC system.

To determine nitrogen dioxide, it was reduced to nitrite whose final concentration was estimated by Griess assay.[26] Briefly, the nitrogen dioxide/nitrogen mixture was burbled into a solution containing an excess of Trolox (500 μM) in phosphate buffer 75 mM, pH 7.4. After 20 min, aliquots (300 μL) were taken and added to a solution (2.6 mL) containing sulphanilamide (1%) in orthophosphoric acid (5%). The solution was incubated at 25 °C for 10 min, and then 100 μL of *N*-(1-naphthyl) ethylenediamine (3%) was added. This solution was incubated at 25 °C for 30 min, and its absorption intensity at 545 nm was measured. Nitrite concentration was determined by comparison with a calibration curve developed with commercial nitrite.

2.2. Spectroscopic Studies. UV−visible spectra of PGR solutions (20 μM) were registered at different pH's in an Agilent 8453 spectrophotometer using different buffers and solutions. A NaCl (0.034 M) solution adjusted with hydrochloric acid to pH 2.0 or 3.0 was employed. Acetate buffer (0.1 M) was used for the pH range between 3.0 and 5.0, while phosphate buffer (75 mM) was employed for the pH range between 5.0 and 8.0. Buffer solutions in the pH range 8.5−11.5 were prepared employing glycine−NaOH buffer (0.1 M). The consumption of PGR induced by RS (AAPH-derived peroxyl radicals, hypochlorite, nitrogen dioxide, and peroxynitrite) was followed by UV−visible spectroscopy. PGR solutions (5−30 μM) in phosphate buffer (75 mM, pH 7.4) were incubated at 37 °C in an UV−visible spectrophotometer (Aligent 8453, Palo Alto, CA, USA) employing a thermostatted cuvette. The reaction was initiated by the addition of the corresponding RS under aerobic conditions, and UV−visible spectra were registered for 30 min.

2.3. Electrochemical Studies. Cyclic voltammetry (CV) experiments were performed in a CH-Instrument electrochemical working station (CHI660C) using a three-electrode configuration. A glassy carbon (GC, CH-Instrument, 0.2 cm in diameter) and a platinum wire were used as working and auxiliary electrodes, respectively. All potentials were measured and reported against a $Ag/AgCl/KCl_{sat}$ reference electrode, provided by CH Instrument. Spectroelectrochemical experiments were carried out employing an UV−vis cuvette with an optical path of 1 cm as the electrochemical cell. A transparent glass slide doped with Sn and In oxides (ITO, 2.45 cm^2 exposed area), purchased from Delta Tec. Ltd., was used as the working electrode. $Ag/AgCl/KCl_{sat}$ and platinum electrodes were used as reference and auxiliary electrodes, respectively. UV−vis and electrochemical data were acquired simultaneously using a Scinco-S-3100 spectrophotometer together with the electrochemical working station. The applied program was a potential double step, in agreement with previous work.[27] Applied potentials were selected from CV experiments, and the

dx.doi.org/10.1021/jp400423w | J. Phys. Chem. B 2013, 117, 4870−4879

Scheme 1

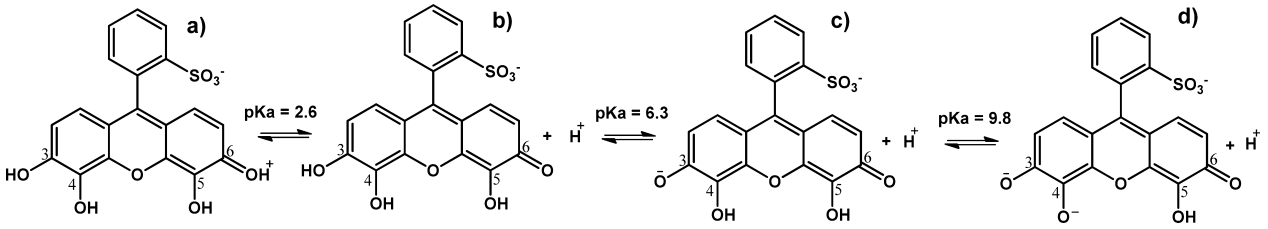

measurements were performed at 25 °C under a nitrogen atmosphere. Absorbance changes were expressed as $\Delta A/A^\circ$ ratios, where $\Delta A = A - A^\circ$ and A° is the absorbance spectrum obtained at open circuit potential. In this analysis, a positive absorbance band indicates the electrochemical formation of a product, while a negative band indicates the consumption of the initial reagent.

2.4. High Performance Liquid Chromatography (HPLC) Studies. The time course of PGR oxidation was followed by HPLC suited with a diode array (HPLC-DAD) and a mass detector (HPLC-MS). HPLC-DAD experiments were carried out employing an Agilent 1200 series HPLC system equipped with a Hibar (Merck) RP-18 (5 μm) column (25 cm × 4.6 mm), and a DAD model G1315D. Potassium dihydrogen phosphate (KH_2PO_4, 0.1 M, adjusted to pH 2.6 with ortophosphoric acid)/acetonitrile (80/20) was employed as the mobile phase (HPLC method A). The flow rate was 0.8 mL/min. Solutions of PGR (5−30 μM) were incubated in the absence and presence of AAPH (10 mM), hypochlorite (15 μM), nitrogen dioxide (3.2 ppm), or peroxynitrite (1 μM) in phosphate buffer, 75 mM at pH 7.4. At different reaction times, aliquots (20 μL) were taken and immediately injected into the HPLC system. The reaction was followed by the consumption of PGR monitored by the decrease in the absorbance at 380 nm. All experiments were carried out in duplicate or triplicate.

The HPLC-DAD-MS/MS analyses were carried out with a Shimadzu HPLC system (Tokio, Japan) equipped with a quaternary LC-10ADVP pump with a FCV-10ALVP elution unit, a DGU-14A degasser unit, a CTO-10AVP oven, and an UV−vis diode array detector (model SPD-M10AVP) coupled in tandem with a QTrap LC/MS/MS 3200 Aplied Biosystems MDS Sciex (California, USA). Instrument control and data collection system were carried out using a CLASS-VP DAD Shimadzu Chromatography Data System and Analyst software (version 1.5.2) for MS/MS analysis.

The analyses were carried out on a C18 column (Kromasil 250 × 4.6 mm, 5 μm) with a C18 precolumn (Nova-Pak Waters, 22 × 3.9 mm, 4 μm) (Milford, MA) at 30 °C. Chromatographic separation condition was an isocratic flow of mobile phase constituted by 75% of formic acid 0.1% in water and 25% acetonitrile, at a flow rate of 0.4 mL min^{-1} (HPLC method B). The sample injection volume was 20 μL, and the column oven temperature was set at 30 °C. Identity assignment was carried out under the following optimized ESI-MS/MS conditions: negative ionization mode, −12 V of collision energy, −4500 V of ionization voltage, capillary temperature at 300 °C and N_2 as nebulization and drying gas at 30 and 25 psi, respectively.

2.5. Quantification of Hydroperoxide Formation. Total hydroperoxides were quantified by FOX's assay.[28] Briefly, 500 μL of PGR solutions (10−30 μM) in the absence and presence of RS was incubated with 4.5 mL of the FOX reagent (0.25 mM ferrous ammonium sulfate and 125 μM xylenol orange (XO) in 25 mM sulfuric acid) for 2 h in an ice bath, after which the absorbance was determined at 560 nm. The concentration of hydroperoxides was determined by preincubating working solutions (500 μL) with 250 μL of catalase (CAT, 11000 U/mL) for 5 min to remove H_2O_2, before analysis. Total hydroperoxide concentrations were determined using a calibration curve generated using commercial H_2O_2, and the data are therefore expressed as H_2O_2 equivalents.

3. RESULTS AND DISCUSSION

3.1. UV−Visible Studies. The chemical structure of PGR contains different groups that, depending on the pH of the medium, are involved in protonation−deprotonation equilibria. pK_a values for PGR of 2.6, 6.3, 9.8, and 11.9 were previously reported.[29] The first pK_a (pK_{a1}) value represents the protonation−deprotonation equilibrium of the carbonyl group at position 6, while the pK_a of 6.3 (pK_{a2}) is related to the hydroxyl group at carbon 3 (Scheme 1). pK_a values of 9.8 and 11.9 (pK_{a3} and pK_{a4}, respectively) are associated with the deprotonation of hydroxyl groups at positions 4 and 5, respectively.

Therefore, dianion c is the dominant species in water at pH 7.4. This species is in equilibrium with mono and trianinon b and d, respectively. These ionic equilibria strongly affect the UV−visible spectrum of PGR. At pH 2.0, PGR presented a visible band with a maximum at 465 nm, whose absorption intensity decreased when the pH of the medium increased (Figure 2). At pH 5.0, the maximum visible band intensity was

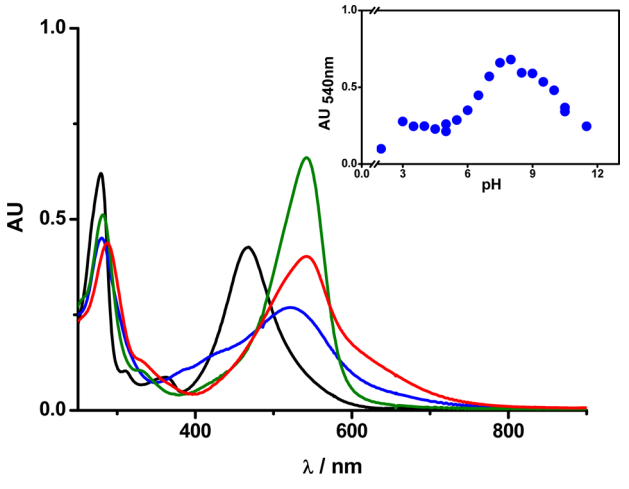

Figure 2. Effect of pH on the UV−visible spectrum of PGR. UV−visible spectra of PGR (20 μM) were measured in aqueous solutions at pH 2.0 (black line), 5.0 (blue line), 7.5 (green line), and 10.0 (red line). The pH's of the solutions were adjusted according to the Experimental Section at 25 °C. Inset: Dependence of the absorption intensity at 540 nm with pH.

dx.doi.org/10.1021/jp400423w | J. Phys. Chem. B 2013, 117, 4870−4879

observed at 526 nm, while, at pH 7.5, the maximum in the absorbance band was evidenced at 540 nm. At pH 8.0, the absorption intensity of this band decreased as the pH of the media increased. From UV−visible experiments (inset, Figure 2), we determined pK_a values in agreement with published data.[29] These results imply that the visible band of PGR at 540 nm at pH 7.4 corresponds to the non-protonated form of the hydroxyl group at carbon 3 (phenolate anion).

The incubation of PGR solutions in phosphate buffer (75 mM, pH 7.4) with reactive species (RS) such as AAPH-derived peroxyl radicals ($ROO^{\bullet}$), hypochlorite (HOCl), superoxide ($O_2^{\bullet-}$), nitrogen dioxide (NO_2), and peroxynitrite ($ONOO^-$) leads to a decrease in the visible absorption band of PGR at 540 nm in concomitance with the formation of a new band in the 390 nm region. This process is characterized by the presence of an isosbestic point at 445 nm, suggesting lack of formation of intermediates. Figure 3 shows a typical result obtained during

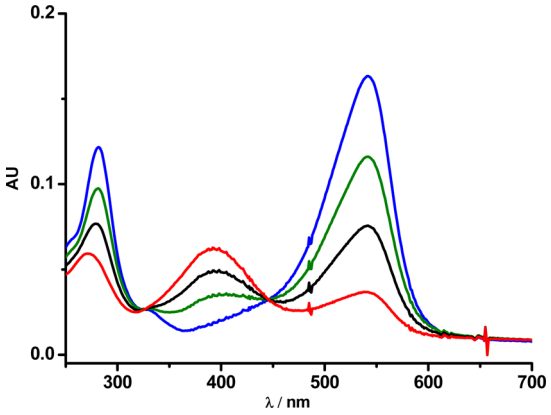

Figure 3. Changes in the UV−visible spectrum of PGR induced by NO_2. Solutions of PGR (5 μM) in phosphate buffer (75 mM, pH 7.4) were burbled with the NO_2/N_2 mixture according with the Experimental Section. Blue, green, black, and red lines: 0, 5, 10, and 20 min of reaction, respectively.

the reaction of PGR with NO_2. The spectroscopic behavior presented in Figure 3 as well as in previously published reports has been associated with a RS-induced oxidation of PGR.[11,13−15] The latter has been supported by spectroscopic data and the stoichiometry of the PGR reaction toward $O_2^{\bullet-}$, $ROO^{\bullet}$, or HOCl, where 2 mol of $ROO^{\bullet}$ or $O_2^{\bullet-}$ consume 1 mol of PGR. The reaction of PGR with HOCl follows a stoichiometry near 1; 1 mol of PGR is consumed by 1 mol of HOCl. In the case of $ONOO^-$, a stoichiometric factor of 0.32 has been reported (Δ[PGR]/Δ[NaOONO]). This value is close to the $ONOO^-$ free radical yield, suggesting that free radicals derived from $ONOO^-$ could be the RS involved in the consumption of PGR.[13]

The similar spectroscopic behavior observed during the consumption of PGR induced by RS of different nature suggests the formation of the same product(s) of reaction. In particular, this point is relevant, since HOCl, NO_2, and $ONOO^-$, in addition to their oxidant capacity, are able to trigger other processes such as chlorination or nitration reactions.[30,31] In addition, similar results have been obtained in the first minutes of PGR consumption mediated by nitrous acid (HONO), a well-known oxidant and nitrosative species (unpublished data).

3.2. Electrochemical Studies. To gain more insights regarding the oxidation of PGR, we carried out electrochemical experiments by cyclic voltammetry (CV) and spectroelectrochemistry. The studies were carried out at different pH in order to evaluate the possible role of protons on the reaction mechanisms associated with the electrochemical PGR oxidation processes.

CV Studies. Cyclic voltammograms were obtained from the open circuit potential in both directions, positive and negative. Figure 4A shows cyclic voltammograms (0.2 V s^{-1}) of the

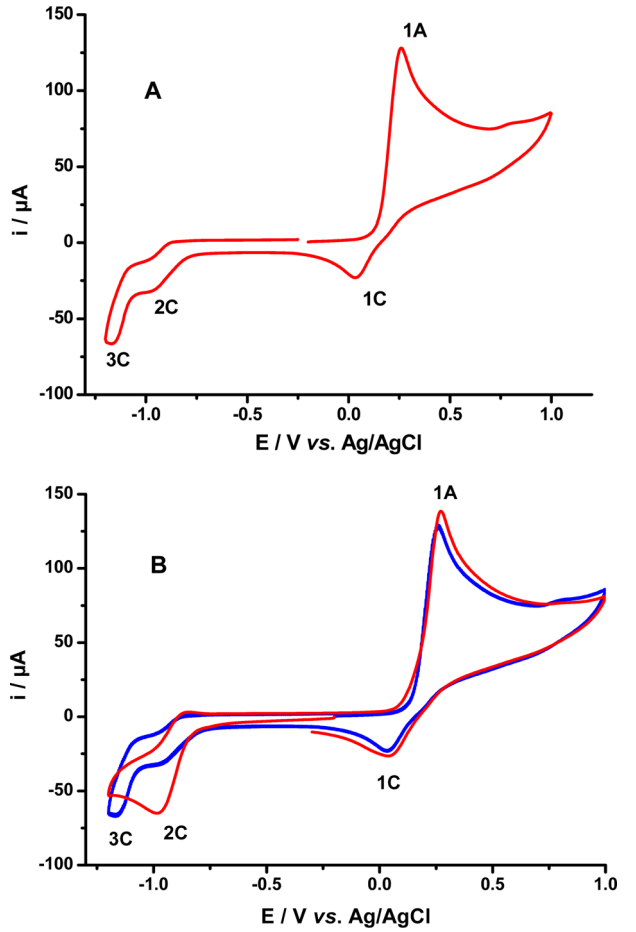

Figure 4. Cyclic voltammograms of PGR in aqueous solutions. Cyclic voltammograms of PGR solutions (5 mM) in phosphate buffer (0.1 M) at pH 8.0. (A) Cyclic voltammogram registered from open circuit potential to positive potential. (B) Cyclic voltammogram registered from open circuit potential to negative potential. First scan = red line; consecutive second scan = blue line. GC was employed as the working electrode, and the scan rate was 0.2 V s^{-1}.

oxidation process (from the open circuit to positive potential) of a 5 mM PGR solution at pH 8 using GC electrode. As this figure shows, PGR is irreversibly oxidized with a peak potential (E_p) near 0.25 V vs Ag/AgCl (peak 1A). A very small peak was observed near 0.00 V corresponding to a reduction process (peak 1C, Figure 4A). The process in peak 1A could be attributed to the formation of a free radical centered in the oxygen atom at carbon 3 which probably is the step controlling the global process.[32] A reversible process (via 1 e^-) would be expected to be involved in the formation of a semiquinone derivative. However, according to the results shown in Figure 4, a low reversibility was observed considering a different potential between both peaks larger than 60 mV. The latter in spite that peak 1C is better resolved at higher potential scan rate at pH 7

dx.doi.org/10.1021/jp400423w | J. Phys. Chem. B 2013, 117, 4870−4879

and 8, where the electro-active species is the enolate[29] and the perturbation is fast. In fact, at pH 4.9, the process at the cathodic peak in the reverse scan is associated with process 2A (see the Supporting Information, Figure 1S). Nevertheless, if the radical is formed, it has diverse possibilities to continue reacting.[32] One of them is the transference of a second electron, forming a quinone, which is evidenced by a reduction process to hydroquinone in the reverse scan; this process would correspond to the cathodic peak 3C (Figure 4B). When voltammograms were first run to negative potentials, from open circuit potential to negative potential, only one reduction process near −1.0 V (peak 2C, Figure 4B) was observed. This peak corresponds to the reduction of pyrogallol red; a consecutive scan shows the process 3C that corresponds to the reduction of the species generated in the anodic process attributed to the quinone compound.

Cyclic voltammograms were very dependent on both the potential scan rate and pH of the electrolyte. Figure 5 presents data obtained at 0.01 (A) and 0.5 (B) V s^{-1} at pH 4.9, 7, and 8. As can be seen in this figure, at both potential scan rates, peak current intensities of all peaks are significantly smaller at pH 4.9 than at pH 7 and 8. This result clearly indicates that the active species is associated with the enolate at position 3 (pK_a = 6.3)

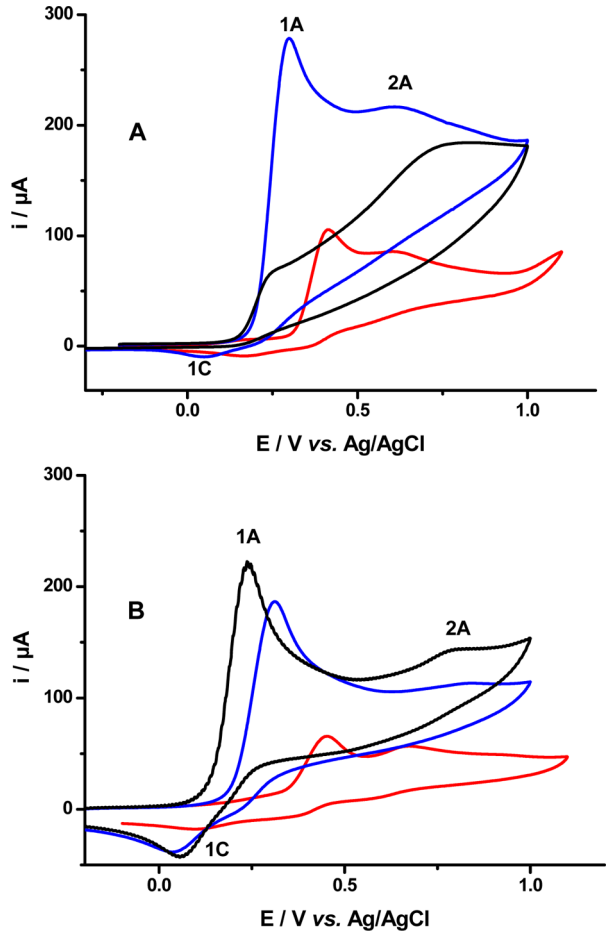

Figure 5. Effect of pH and scan rate on cyclic voltammograms of PGR. Cyclic voltammograms of PGR solutions (5 mM) were registered at 0.01 (A) and 0.5 (B) V s^{-1} at pH 4.9, 7, and 8 (red, blue, and black curves, respectively). Cyclic voltammograms were registered in phosphate buffer (0.1 M) from open circuit potential to positive potential employing GC as the working electrode.

of the PGR chemical structure, and that the acid−base equilibrium is slow. The observed dependence of E_p with pH (see the Supporting Information, Figure 2S) is in agreement with the fact that at pH 4.9 there is one hydrogen atom transferred in a chemical reaction coupled to the charge transfer process. A second anodic process (peak 2A, Figure 5A) is observed at low potential scan rate (0.01 V s^{-1}), while at 0.5 V s^{-1} at pH 7 and 8 a higher reversibility degree of peak current in 1C in comparison with a scan rate of 0.01 V s^{-1} (Figure 5B) was observed.

The analysis of the results obtained with CV at different potential sweep rates (between 0.5 and 0.01 V s^{-1}) is presented in the Supporting Information. From the plots of peak potential against the potential scan rate is estimated the peak potential at 1 mV s^{-1} ($E_p°$), which is plotted versus the pH in Figure 2S (Supporting Information). The potential is shifted to less positive potential with the increase in pH in agreement with a change in the active species. The latter can be explained considering that, at pH values lower than pK_{a2} (pK_a of hydroxyl group at position 3), the rate of the enolate formation is slow, involving a determinant chemical step upon the rate of the overall process.

The oxidation process behaves as an irreversible process under diffusion control with

$$j_p = (2.99 \times 10^5) n(\alpha n_\alpha)^{0.5} C^* D^{0.5} \nu^{0.5} \quad (1)$$

Equation 1 describes the dependence of peak current (j_p in A cm^{-2}) of an irreversible process under diffusion control (j_p vs $\nu^{1/2}$ linear). In this equation, n is the number of electrons involved in the overall electrode reaction; α is the transfer coefficient; and n_α is the number of electrons transferred up to, and including, the rate determining step. D is the diffusion coefficient in cm^2 s^{-1}, and C^* is the PGR concentration (mol cm^{-3}). In consequence, a linear plot between j_p against the square root of the potential scan rate is expected (Figure 2S, Supporting Information). At pH 4.9, the $dI_p/d\nu^{0.5}$ slope is considerably lower, whereas, at pH 8, a change in slope is observed which probably can be a consequence that at this pH the reaction product seems to be in the vicinity of an acid−base (pK_a) equilibrium, which affects the concentration of the reactive species. This behavior can be due to a change in the electrochemical mechanism with the potential scan rate as a consequence of a variation on the reactive species. In fact, at pH 8, there is a small fraction of the deprotonated hydroxyl group at position 4 (pK_{a3} = 9.8) that can modify the oxidation mechanism observed for main species present at pH 7 (see Scheme 1).

Thus, the dissociation equilibrium associated with pK_{a2} (Scheme 1) plays an important role in the global electrochemical reaction. We postulate that the electrochemical reaction begins with the formation of a phenoxy radical (by loss of one electron in the oxygen at carbon 3) that quickly forms the phenoxyradical, which after a second charge transfer reaction (loss of a second electron) generates an ortho-quinone derivative (Scheme 2).

Spectroelectrochemical Studies. The chronoamperometry technique, especially employing an ITO electrode, is a powerful tool to study, by the spectroelectrochemical method, systems involving coupled chemical and redox reactions. In addition, cyclic voltammograms obtained at the ITO surface are very similar to those obtained employing a GC electrode, supporting a comparison between spectro-electrochemical and CV results.

dx.doi.org/10.1021/jp400423w | J. Phys. Chem. B 2013, 117, 4870−4879

Scheme 2

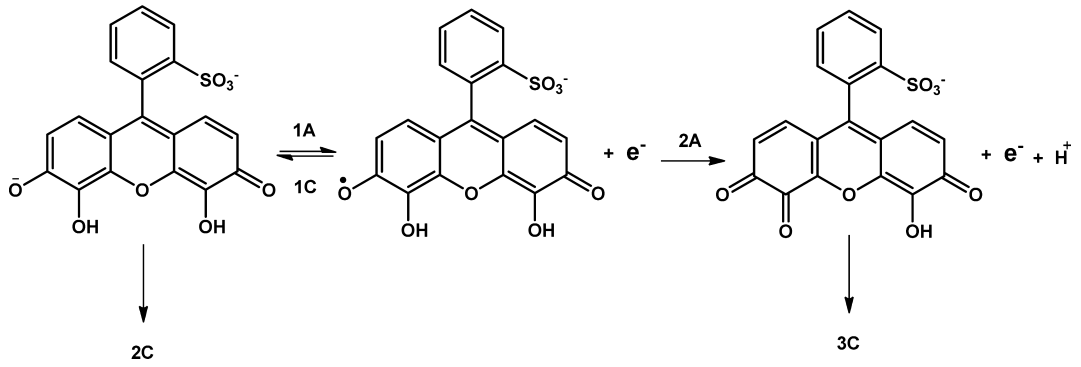

In our experiments, the open circuit potential was employed as the initial potential, which was instantaneously changed to the potential of peak 1A (positive, Figure 4) during 60 s. After that period of time, the potential was changed in the negative direction to the potential of process 2C (Figure 4B). Both, the time course of the current and UV−visible spectra (acquired employing an ultrafast UV−vis spectrophotometer) were continuously registered.

PGR solutions (600 μM) in phosphate buffer (0.1 M) at pH 5.2, 7, and 8 were studied by the spectroelectrochemistry technique. The initial spectrum (at open circuit potential, $A°$) was registered as well as differential UV−visible spectra ($(A - A°)/A°$). The latter spectra were plotted as a function of the time. In this type of plots, a positive band is related to the appearance of new species, whereas a negative band is associated with the decrease of the UV−visible spectrum of the original reactant (PGR).

As shown in Figure 6, the application of the potential corresponding to peak 1A induced changes in the UV−visible spectrum of PGR. These changes involved the decrease of the original band of PGR (at 540 nm) together with the generation of a new band (positive) at 390 nm and an isosbestic point at 445 nm. This behavior was evidenced at pH 7 and 8, while at pH 5.2 the spectrum of PGR was slightly modified. Both the formation of a new band at 390 nm and the decrease at 540 nm agree with the processes related to the PGR-RS reaction, as is presented in Figure 3.

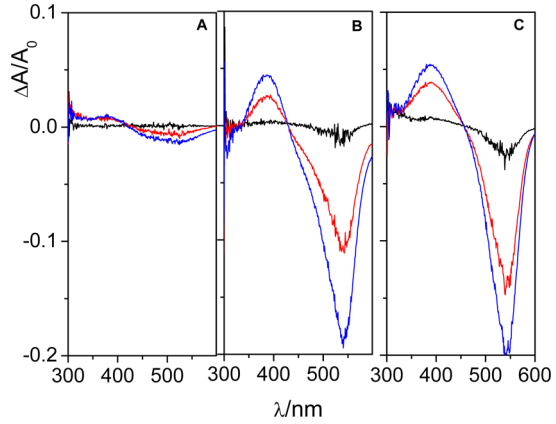

Figure 6. *In situ* changes in the differential UV−visible spectra of PGR induced by a potential application. Differential spectra of PGR solutions (50 μM) were obtained during the application of a potential step from 0.2 to E^+/V at pH 5.2 (A), 7 (B), and 8 (C). An ITO electrode was employed as the working electrode. Spectra 1, 5, and 9: black, red, and blue, respectively.

As a whole, the above presented results highlight the following points:

- Independently of the oxidant (peroxyl radicals, hypochlorite, nitrogen dioxide, peroxynitrite, or electrochemical techniques), the oxidation of PGR leads to the same changes in the UV−visible spectrum.
- The results obtained by spectroelectrochemistry indicate that the processes at pH 7 and 8 were the same as those at pH 5.2 (Figure 6). The difference in the obtained UV−visible spectra could be attributed to a decrease in the rate of the electrochemical reaction at pH 5.2. This result is in agreement with the results obtained by CV (Figure 5).
- Interestingly, when after the application of the potential program above described was applied a second potential step at negative potential, no changes were observed in the UV−visible spectrum, indicating the occurrence of an irreversible oxidation process.

From the integration of the current−time curves registered during the potential step were obtained the electrical charge associated to the process (Q), as a time function.[27] According to the correlation given by eq 2,

$$|Q| = \frac{4nFk}{\pi}[C]°(t_L^{0.5}t^{0.5} - t_L) \quad (2)$$

where k is the heterogeneous rate constant, $t_L^{0.5}$ is the intercept on the x-axis, and t_L is a constant. Therefore, from a Q versus $t^{0.5}$ plot, it is possible to estimate the value of the rate constant associated with the electrodic process. Kinetic rate constants for the electro-oxidation process (k_{1A}), estimated from data depicted in Figure 7, are 0.256, 0.526, and 0.305 cm s^{-1} at pH 5.2, 7.0, and 8.0, respectively, and are in agreement with the CV results in terms of the process associated with peak 1A shown in Figure 4.

3.3. High Performance Liquid Chromatography (HPLC) Studies. To study the product(s) generated during the PGR reaction with RS, HPLC assays were carried out. Figure 8 shows the chromatographic results obtained from a PGR solution in the absence and after treatment with $ROO^•$, HOCl, NO_2, or $ONOO^-$. As shown, the presence of these RS induces a decrease in the area of the chromatographic peak of PGR (registered at 11 min, employing HPLC method A) together with the formation of two new peaks at 5.2 and 5.6 min. These results imply that, independently of the RS employed, two products were generated (in the first reaction

dx.doi.org/10.1021/jp400423w | J. Phys. Chem. B 2013, 117, 4870−4879

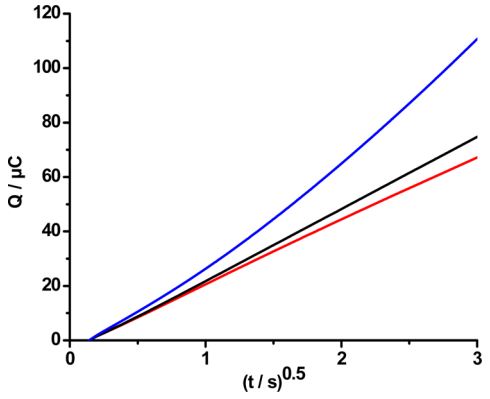

Figure 7. Chronocoulometry experiments: charge dependence with $t^{0.5}$. Chronocoulometry data were obtained by applying potential step from 0.2 V to a positive potential (E^+) at pH 5.2 (red line), 7.0 (black line), and 8.0 (blue line).

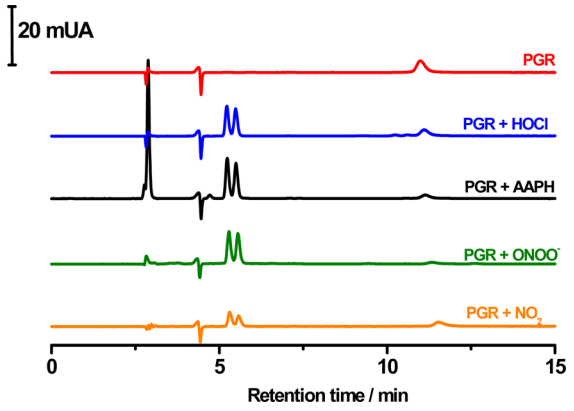

Figure 8. Time course of the reaction of PGR with RS followed by HPLC-DAD. PGR solutions (15 μM) were incubated in the absence (red line) or presence of RS in phosphate buffer at pH 7.4. Black and orange lines: Chromatograms obtained after 10 min of PGR incubation with 10 mM AAPH or NO_2 (3.2 ppm), respectively. Blue and green lines represent chromatograms obtained after 5 min of PGR incubation with HOCl (10 μM) and $ONOO^-$ (1 μM), respectively. Chromatograms were obtained (λ = 380 nm) and solutions were incubated in phosphate buffer (pH 7.4) at 37 °C.

times) during the oxidative consumption of PGR. Interestingly, the chromatographic peaks, associated with these products, showed identical UV−visible spectra (Figure 9), suggesting that both products have very similar chemical structures.

To study the identity of the latter, HPLC with mass detection was used. As is presented in Figure 10A, the fragmentation pattern of the chromatographic peak of PGR (registered at 13.5 min employing HPLC method B) is in agreement with the structure of PGR (ion molecular = 399 m/z). In addition, a MS^2 analysis of the fragment at 399 m/z showed a second fragmentation with m/z = 320, which could be explained by the loss of the sulfonic moiety of PGR (Figure 10B). Employing HPLC method B, the products of the PGR-RS reaction showed chromatographic peaks at 10.2 and 10.5 min. Both peaks present the same fragmentation pattern, which includes the fragments m/z = 433, 389, and 361 (Figure 11). In addition, the MS^2 pattern of 433 m/z showed the formation of fragments 389 and 361, implying a relationship between all the fragments registered. Considering these results and the fact that both peaks presented the same UV−visible spectra, we estimate

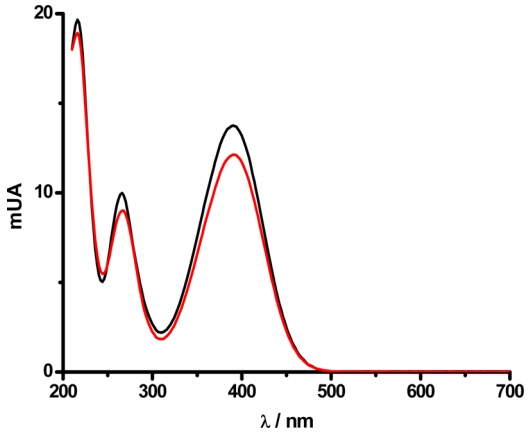

Figure 9. UV−visible spectra of HPLC peaks generated during the PGR-RS incubation. UV−visible spectra of the HPLC peaks at 5.6 min (red line) and 5.1 min (black line) obtained after 15 min of the PGR (15 μM) incubation with AAPH (10 mM) in phosphate buffer 75 mM, pH 7.4 at 37 °C. Spectra recorded in the HPLC analysis using KH_2PO_4, 0.1 M, adjusted to pH 2.6 with ortophosphoric acid)/ acetonitrile (80/20) employed as the mobile phase.

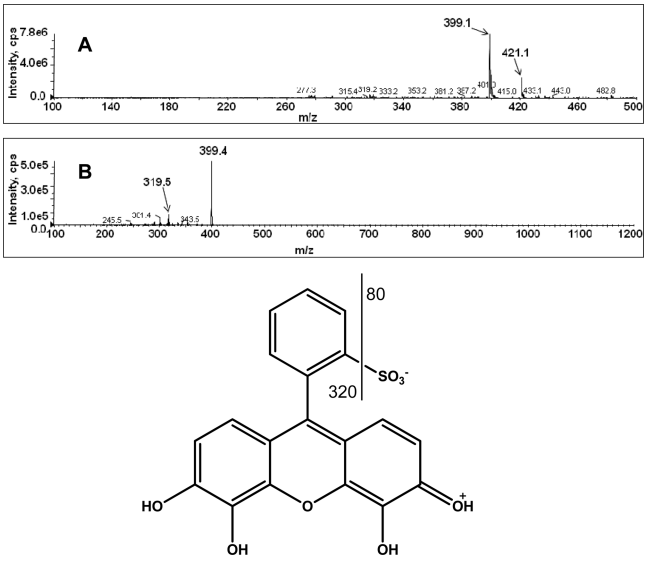

Figure 10. Extracted mass spectra (HPLC-MS) of PGR. (A) Mass spectrum of the HPLC-MS peak (13.5 min) corresponding to a PGR (15 μM) solution in phosphate buffer 75 mM, pH 7.4. (B) Extracted mass spectrum (MS^2) of the fragment at 399 m/z presented in part A. HPLC-MS experiments were carried out employing the experimental conditions described in the Experimental Section (HPLC method B). This figure also presents the proposed fragmentation pattern of PGR.

that the chromatographic peaks are associated with the presence of isomers of a single product formed during the reaction (in our experimental conditions) of PGR with RS.

The formation of the m/z = 433 could be explained by the generation of organic peroxides during the reaction of PGR with RS or by the formation of a quinone derivative interacting with chloride ions into the mass detector. To gain insights regarding the first possibility, we carried out experiments aimed at determining hydroperoxides (throughout Fox's assay) during the reaction of PGR and AAPH-derived peroxyl radicals at 37 °C.[28] Control solutions (containing only PGR or AAPH) evidenced the presence of hydroperoxides at very low concentrations (1−3 μM). The addition of in-excess catalase

dx.doi.org/10.1021/jp400423w | J. Phys. Chem. B 2013, 117, 4870−4879

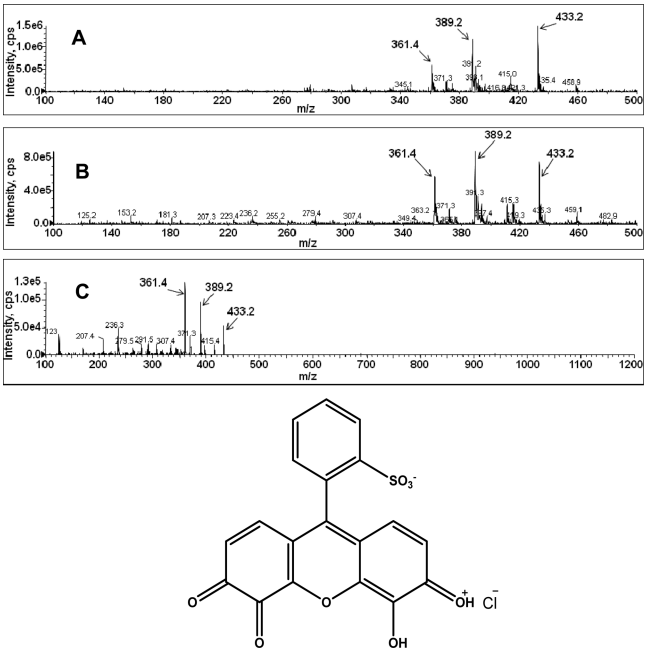

Figure 11. Extracted mass spectrum (HPLC-MS) of the products of the reaction between PGR and RS. Mass spectra of the HPLC-MS peaks at 10.2 and 10.6 min; Parts A and B, respectively, were obtained after 5 min of the PGR (15 μM) reaction with HOCl (10 μM). Part C shows the extracted mass spectrum (MS^2) of the fragment at 433 m/z presented in parts A and B. HPLC-MS experiments were carried out employing the experimental conditions described in the Experimental Section (HPLC method B). This figure also presents the proposed fragmentation pattern of products.

to PGR-AAPH solutions did not modify hydroperoxide concentrations, discarding the presence of hydrogen peroxide. As Figure 12 shows, during the incubation of such solutions, the formation of hydroperoxides increased linearly in a time-dependent way (rate = 0.6 μM/min). No effect of the PGR concentration was evidenced, since similar concentrations of

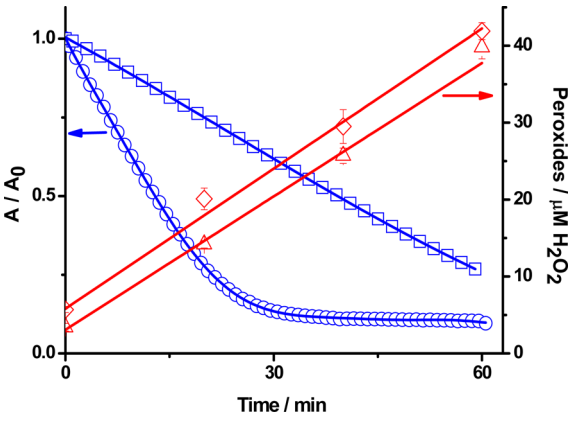

Figure 12. Formation of hydroperoxides during the reaction of PGR with AAPH-derived peroxyl radicals. PGR solutions (10 (○) or 30 (□) μM) were incubated with AAPH (10 mM) at 37 °C in phosphate buffer 75 mM, pH 7.4, and the reaction followed at 540 nm (blue symbols). Every 20 min, aliquots were taken and the hydroperoxide concentration was analyzed by Fox's assay. Red symbols: hydroperoxides formed in the presence of AAPH (10 mM) and PGR at 10 (△) and 30 μM (◇). Hydroperoxide concentration (right axis) were expressed in hydrogen peroxide equivalents (μM).

hydroperoxides were generated at PGR 10 and 30 μM. Interestingly, at a 10 μM PGR concentration, hydroperoxides were generated even when practically all PGR was consumed. This fact would reflect the ability of the oxidized products of PGR to further react with AAPH-derived peroxyl radicals. Taking into account that the formation of peroxides during the PGR-RS reaction could be associated with a consumption of oxygen, we followed the oxygen concentration during such reactions. If hydroperoxides are being formed from reactions

$$\text{AAPH} \xrightarrow{O_2} \text{ROO}^{\bullet} \quad \text{(R1)}$$

$$\text{PGR} + \text{ROO}^{\bullet} \rightarrow \text{PGR}(-\text{H})^{\bullet} + \text{ROOH} \quad \text{(R2)}$$

$$2\text{PGR}(-\text{H})^{\bullet} \rightarrow \text{PGR} + \text{Quinone} \quad \text{(R3)}$$

$$\text{PGR}(-\text{H})^{\bullet} + \text{ROO}^{\bullet} \rightarrow \text{ROOH} + \text{Quinone} \quad \text{(R4)}$$

$$2\text{ROO}^{\bullet} \rightarrow \text{ROOR} + \text{O}_2 \quad \text{(R5)}$$

it is expected that a solution containing PGR plus AAPH presents higher oxygen consumption than the consumption associated only for the AAPH decomposition (reaction R1). Nonetheless, the addition of PGR (120 μM) to a solution of AAPH (10 mM, incubated at 37 °C) did not modify the consumption of oxygen associated with the generation of $ROO^{\bullet}$ by AAPH (see Figure 3S, Supporting Information). In addition, the rate of hydroperoxide formation (0.6 μM/min, Figure 12) is in the same order as the rate of the peroxyl radical formation from AAPH (0.8 μM/min), suggesting that hydroperoxides are associated with the formation of ROOH in reactions R2 and R4.[33] The latter is also supported by the fact that PGR solutions in the presence of hypochlorite (instead AAPH) revealed no formation of hydroperoxides (data not shown). Furthermore, the interaction of hypochlorite with PGR in a free oxygen atmosphere led to the same chromatographic profile as that presented in Figure 8. Therefore, we consider that these results strongly support the interpretation that the m/z = 433 fragment is not related to the formation of hydroperoxydes on the PGR molecule. Considering the latter and the fact that this fragment presents the isotope chloride distribution, we estimate that such a fragment could be explained by the interaction of chloride ions with a quinone derivative generated as product during the PGR-RS reaction (Figure 11).

4. CONCLUSIONS

In the present study, we have demonstrated that the reaction of PGR with several oxidants, such as peroxyl radicals, hypochlorite, nitrogen dioxide, or peroxinitrite, renders almost quantitatively a single product. The spectroscopic properties of this product and its mass analysis indicate that this product corresponds to a quinone derivative. These results are in full agreement with the electrochemical oxidation of PGR and the spectroelectrochemical data, where the quinone product is formed from an initial phenoxyl radical, mainly from the deprotonated enolate species of PGR, and consecutive electron transfer. These results suggest that, in spite of oxidants like hypochlorite, nitrogen dioxide, or peroxinitrite that may produce chlorination or nitration, only oxidation of PGR is observed, and then, inhibition of PGR degradation by substrates mainly protect from the oxidation process.

dx.doi.org/10.1021/jp400423w | J. Phys. Chem. B 2013, 117, 4870−4879

■ ASSOCIATED CONTENT

Supporting Information

Supplementary Figure S1: Effect of the positive potential limit evaluated at pH 4.9 on the electrodic response of a 5 mM PGR solution using GC electrode at 0.1 V s^{-1}. Supplementary Figure S2: Effect of pH and potential scan rate on the oxidation process (peak 1A) of PGR (5 mM) employing GC electrode. Supplementary Figure S3: Oxygen consumption mediated by the AAPH decomposition in the absence and presence of PGR. This material is available free of charge via the Internet at http://pubs.acs.org.

■ AUTHOR INFORMATION

Corresponding Author

*E-mail: clopezr@uc.cl (C.L.-A.); alexis.aspee@usach.cl (A.A.).

Notes

The authors declare no competing financial interest.

■ ACKNOWLEDGMENTS

We are grateful to FONDECYT (grants 1100659, 1110809, and 1100476) for financial support. Elias Atala gratefully acknowledges CONICYT fellowship (Chilean Commission of Scientific Research and Technology, 24121097).

■ REFERENCES

(1) Behr, S.; Trumel, C.; Palanche, F.; Braun, J. P. Assessment of a Pyrogallol Red Technique for Total Protein Measurement in the Cerebrospinal Fluid of Dogs. *J. Small Anim. Pract.* **2003**, *44*, 530−533.

(2) Higby, K.; Suiter, C. R.; Silerkhodr, T. A Comparison between Two Screening Methods for Detection of Microproteinuria. *Am. J. Obstet. Gynecol.* **1995**, *173*, 1111−1114.

(3) Arancibia, V.; Munoz, C. Determination of Aluminium in Water Samples by Adsorptive Cathodic Stripping Voltammetry in the Presence of Pyrogallol Red and a Quaternary Ammonium Salt. *Talanta* **2007**, *73*, 546−552.

(4) Ensafi, A. A.; Khayamian, T.; Atabati, M. Differential Pulse Cathodic Stripping Adsorption Voltammetric Determination of Trace Amounts of Lead Using Factorial Design for Optimization. *Talanta* **2003**, *59*, 727−733.

(5) Ensafi, A. A.; Khayamian, T.; Khaloo, S. S. Application of Adsorptive Cathodic Differential Pulse Stripping Method for Simultaneous Determination of Copper and Molybdenum Using Pyrogallol Red. *Anal. Chim. Acta* **2004**, *505*, 201−207.

(6) Rojas, C.; Arancibia, V.; Gomez, M.; Nagles, E. Adsorptive Stripping Voltammetric Determination of Cobalt in the Presence of Nickel and Zinc Using Pyrogallol Red as Chelating Agent. *Int. J. Electrochem. Sci.* **2012**, *7*, 979−990.

(7) Ensafi, A. A.; Rezaei, B. Kinetic-Spectrophotometric Determination of Traces of Osmium by Its Catalytic Effect on the Oxidation of Pyrogallol Red by Hydrogen Peroxide. *Anal. Lett.* **1993**, *26*, 1771−1785.

(8) Ensafi, A. A.; Haghighi, A. Spectrophotometric Reaction Rate Method for the Determination of Molybdenum by its Catalytic Effect on the Oxidation of Pyrogallol Red with Hydrogen Peroxide. *Fresenius' J. Anal. Chem.* **1998**, *360*, 535−538.

(9) Ensafi, A. A.; Keyvanfard, M. Kinetic-Spectrophotometric Determination of Palladium in Hydrogenation Catalyst by Its Catalytic Effect on the Oxidation of Pyrogallol Red by Hydrogen Peroxide. *Spectrochim. Acta, Part A* **2002**, *58*, 1567−1572.

(10) Ensafi, A.; Mirmomtaz, E. Electrocatalytic Oxidation of Hydrazine with Pyrogallol Red as a Mediator on Glassy Carbon Electrode. *J. Electroanal. Chem.* **2005**, *583*, 176−183.

(11) Lopez-Alarcon, C.; Lissi, E. Interaction of Pyrogallol Red With Peroxyl Radicals. A Basis for a Simple Methodology for the Evaluation of Antioxidant Capabilities. *Free Radical Res.* **2005**, *39*, 729−736.

(12) Niki, E. Assessment of Antioxidant Capacity in Vitro and in Vivo. *Free Radical Biol. Med.* **2010**, *49*, 503−515.

(13) Balavoine, G. G. A.; Geletii, Y. V. Peroxynitrite Scavenging by Different Antioxidants. Part I: Convenient Assay. *Nitric Oxide* **1999**, *3*, 40−54.

(14) Faundez, M.; Rojas, M.; Bohle, P.; Reyes, C.; Letelier, M. E.; Aliaga, M. E.; Speisky, H.; Lissi, E.; Lopez-Alarcon, C. Pyrogallol Red Oxidation Induced by Superoxide Radicals: Application to Evaluate Redox Cycling of Nitro Compounds. *Anal. Biochem.* **2011**, *419*, 284−291.

(15) Lopez-Alarcon, C.; Lissi, E. A Novel and Simple ORAC Methodology Based on the Interaction of Pyrogallol Red with Peroxyl Radicals. *Free Radical Res.* **2006**, *40*, 979−985.

(16) Robaszkiewicz, A.; Bartosz, G. Estimation of Antioxidant Capacity Against Pathophysiologically Relevant Oxidants Using Pyrogallol Red. *Biochem. Biophys. Res. Commun.* **2009**, *390*, 659−661.

(17) Alarcon, E.; Campos, A. M.; Edwards, A. M.; Lissi, E.; Lopez-Alarcon, C. Antioxidant Capacity of Herbal Infusions and Tea Extracts: A Comparison of ORAC-Fluorescein and ORAC-Pyrogallol Red Methodologies. *Food Chem.* **2008**, *107*, 1114−1119.

(18) Atala, E.; Vasquez, L.; Speisky, H.; Lissi, E.; Lopez-Alarcon, C. Ascorbic Acid Contribution to ORAC Values in Berry Extracts: An Evaluation by the ORAC-Pyrogallol Red Methodology. *Food Chem.* **2009**, *113*, 331−335.

(19) Omata, Y.; Yoshida, Y.; Niki, E. Assessment of the Antioxidant Capacity of Natural Fruit Extracts by Inhibition of Probe Decay and Plasma Lipid Peroxidation. *Biosci., Biotechnol., Biochem.* **2010**, *74*, 531−535.

(20) Torres, P.; Galleguillos, P.; Lissi, E.; Lopez-Alarcon, C. Antioxidant Capacity of Human Blood Plasma and Human Urine: Simultaneous Evaluation of the ORAC Index and Ascorbic Acid Concentration Employing Pyrogallol Red as Probe. *Bioorg. Med. Chem.* **2008**, *16*, 9171−9175.

(21) Omata, Y.; Ogawa, Y.; Saito, Y.; Yoshida, Y.; Niki, E. Assessment of the Antioxidant Capacity of a Fermented Grain Food Product, Antioxidant Biofactor (AOB), by Using Pyranine and Pyrogallol Red as a Combined Probe. *Food Chem.* **2009**, *114*, 429−433.

(22) Omata, Y.; Saito, Y.; Yoshida, Y.; Niki, E. Simple Assessment of Radical Scavenging Capacity of Beverages. *J. Agric. Food Chem.* **2008**, *56*, 3386−3390.

(23) Takashima, M.; Shichiri, M.; Hagihara, Y.; Yoshida, Y.; Niki, E. Reactivity toward Oxygen Radicals and Antioxidant Action of Thiol Compounds. *Biofactors* **2012**, *38*, 240−248.

(24) Saha, A.; Goldstein, S.; Cabelli, D.; Czapski, G. Determination of Optimal Conditions for Synthesis of Peroxynitrite by Mixing Acidified Hydrogen Peroxide with Nitrite. *Free Radical Biol. Med.* **1998**, *24*, 653−659.

(25) Buldt, A.; Karst, U. *Anal. Chem.* **1997**, *69*, 3617−3622.

(26) Tsikas, D.; Fuchs, I.; Gutzki, F. M.; Frolich, J. C. Measurement of Nitrite and Nitrate in Plasma, Serum and Urine of Humans by High-Performance Liquid Chromatography, the Griess Assay, Chemiluminescence and Gas Chromatography-Mass Spectrometry: Interferences by Biogenic Amines and N(G)-nitro-L-arginine Analogs. *J. Chromatogr., B: Biomed. Sci. Appl.* **1998**, *715*, 441−444.

(27) Velasquez, G.; Ureta-Zanartu, M. S.; Lopez-Alarcon, C.; Aspee, A. Electrochemical and Spectroscopic Study of Pyranine Fluorescent Probe: Role of Intermediates in Pyranine Oxidation. *J. Phys. Chem. B* **2011**, *115*, 6661−6667.

(28) Bou, R.; Codony, R.; Tres, A.; Decker, E. A.; Guardicila, F. Determination of Hydroperoxides in Foods and Biological Samples by the Ferrous Oxidation-Xylenol Orange Method: A Review of the Factors That Influence the Method's Performance. *Anal. Biochem.* **2008**, *377*, 1−15.

(29) Ivanov, V. M.; Mamedov, A. M. 3,4,5-Trihydroxyfluorones as Analytical Reagents. *J. Anal. Chem.* **2006**, *61*, 1040−1062.

(30) Deborde, M.; von Gunten, U. Reactions of Chlorine with Inorganic and Organic Compounds during Water Treatment-Kinetics and Mechanisms: A Critical Review. *Water Res.* **2008**, *42*, 13−51.

(31) Nonoyama, N.; Oshima, H.; Shoda, C.; Suzuki, H. The Reaction of Peroxynitrite with Organic Molecules Bearing a Biologically Important Functionality. The Multiplicity of Reaction Modes as Exemplified by Hydroxylation, Nitration, Nitrosation, Dealkylation, Oxygenation, and Oxidative Dimerization and Cleavage. *Bull. Chem. Soc. Jpn.* **2001**, *74*, 2385−2395.
(32) Hodnick, W. F.; Milosavljevic, E. B.; Nelson, J. H.; Pardini, R. S. Electrochemistry of Flavonoids. Relationships Between Redox Potentials, Inhibition of Mitochondrial Respiration, and Production of Oxygen Radicals by Flavonoids. *Biochem. Pharmacol.* **1988**, *37*, 2607−2611.
(33) Niki, E. Free Radical Initiators as Source of Water- or Lipid-Soluble Peroxyl Radicals. *Methods Enzymol.* **1990**, *186*, 100−108.